

Numerical modelling of bottom-hole rock in underbalanced drilling using thermo-poroelastoplasticity model

Weiji Liu^{1,2}, Yunlai Zhou², Xiaohua Zhu¹, Xiannan Meng², Mei Liu³ and Magd Abdel Wahab^{*4,5,6}

¹School of Mechatronic Engineering, Southwest Petroleum University, 610500, Chengdu, China

²Department of Civil and Environmental Engineering, National University of Singapore, 117576, Singapore

³Guangdong Provincial Key Laboratory of Durability for Marine Civil Engineering, Shenzhen University, Shenzhen 518060, China

⁴Division of Computational Mechanics, Ton Duc Thang University, Ho Chi Minh City, Vietnam

⁵Faculty of Civil Engineering, Ton Duc Thang University, Ho Chi Minh City, Vietnam

⁶Soete Laboratory, Faculty of Engineering and Architecture, Ghent University, Technologiepark Zwijnaarde 903, Zwijnaarde B-9052, Belgium

(Received June 22, 2018, Revised January 22, 2019, Accepted January 25, 2019)

Abstract. Stress analysis of bottom-hole rock has to be considered with much care to further understand rock fragmentation mechanism and high penetration rate. This original study establishes a fully coupled simulation model and explores the effects of overburden pressure, horizontal in-situ stresses, drilling mud pressure, pore pressure and temperature on the stress distribution in bottom-hole rock. The research finds that in air drilling, as the well depth increases, the more easily the bottom-hole rock is to be broken. Moreover, the mud pressure has a great effect on the bottom-hole rock. The bigger the mud pressure is, the more difficult to break the bottom-hole rock is. Furthermore, the maximum principal stress of the bottom-hole increases as the mud pressure, well depth and temperature difference increase. The bottom-hole rock can be divided into three main regions according to the stress state, namely a) three directions tensile area, b) two directions compression areas and c) three directions compression area, which are classified as a) easy, b) normal and c) hard, respectively, for the corresponding fragmentation degree of difficulty. The main contribution of this paper is that it presents for the first time a thorough study of the effect of related factors, including stress distribution and temperature, on the bottom-hole rock fracture rather than the well wall, using a thermo-poroelastoplasticity model.

Keywords: thermo-poroelastoplasticity; bottom-hole rock stress; fully coupled analysis; finite element analysis; fragmentation mechanism

1. Introduction

The rock drilling ability becomes worse with the petroleum exploration and development towards the deep and ultra-deep formations. Consequently, the rate of penetration (ROP) sharply is reduced causing increase in the drilling costs. The underbalanced drilling as a relatively new technology has many advantages such as high drilling efficiency, low cost, protecting the oil and gas reservoir. These advantages make it been used in oil gas drilling extensively, especially for the hard formation drilling. The stress field in the bottom hole rock has a close relationship with the high drilling efficiency of underbalanced drilling. Hence, it is significant to investigate the stress distribution of bottom-hole rock for a good understanding of the rock fragmentation mechanism and high ROP. The stress distribution is very complicated because it involves the combination of overburden pressure, horizontal in-situ stresses, drilling mud pressure, pore pressure and temperature.

In the past decades, many researchers have paid much attention to the stability of the borehole in underbalanced drilling. However, the stress distribution of bottom-hole rock under unbalanced drilling is still lacking deep investigation. Mclellan and Hawkes (2001) have employed the software STABViewTM to forecast the optimum bottom-hole pressure in underbalanced drilling. Salehi *et al.* (2007, 2010) used the elastic-plastic model and finite-explicit and finite element method (FEM) to explore the wellbore instability problems in underbalanced drilling in depleted Iranian fields. Azeemuddin *et al.* (2006) constructed a geomechanical model to assess the optimal mud weights in underbalanced drilling. Roshan and Rahman (2011) constructed a three-dimensional (3D) wellbore model to obtain the optimal mud composition and a certain range of bottom hole pressure in underbalanced drilling. Qiu *et al.* (2008) discussed a wellbore stability analysis to assess the potential wellbore instability risk with UBD. Aminul *et al.* (2009a, 2009b) explored the hidden problems resulting in wellbore instability in underbalanced drilling in shale. He *et al.* (2014) derived a new wellbore collapse pressure model based on seepage mechanics and linear elastic theory and a new analytical model that took fluid seepage into consideration to examine wellbore circumferential stresses. The high drilling efficiency and low cost of underbalanced drilling has been widely recognized by engineers

*Corresponding author

E-mail: magd.abdelwahab@tdt.edu.vn or
magd.abdelwahab@ugent.be

(Shirkavand *et al.* 2009). Some studies on stress distribution of bottom-hole rock in underbalanced drilling have been conducted as follows. Rumzan and Schmitt (2001), Zhuang *et al.* (2014) established 3D finite element (FE) model of bottom-hole rock and investigated the stress state under various mud pressure. Zhang *et al.* (2012), Li *et al.* (2014) analyzed the stress state of bottom-hole rock under different mud pressure and temperature and the rock failure mechanism also was elaborated. Amadi *et al.* (2012) studied the stress state of bottom-hole rock before drilling, during drilling and after drilling based on the excavation method. Li *et al.* (2011) employed FEM to investigate the influence mechanism imposed by pore pressure and temperature of strata on the stress state of bottom-hole rock. Bezminabadi *et al.* (2017), Zhang *et al.* (2013), Chang *et al.* (2014), Li *et al.* (2016), established the fluid-solid coupling model with the bottom-hole differential pressure, and used FEM to compute the bottom-hole stress field under differential pressures. Nguyen *et al.* (2017) reviewed the problem of computational modelling of a fluid-driven fracture propagating in a permeable porous medium using zero-thickness flow cohesive interface elements. Rabczuk and Ren (2017) presented a dual-horizon peridynamics (DH-PD) formulation for fracture in granular and rock-like materials. The pre-holed concrete Brazilian disc specimens are numerically modelled by a two-dimensional discrete element approach, the cracks initiation, propagation and coalescence in the numerically simulated Brazilian discs are studied (Sarfarazi *et al.* 2018). Zhou *et al.* (2018a, 2018b) presented a phase field model (PFM) for simulating complex crack patterns including crack propagation, branching and coalescence in rock. Other related applications focused on using numerical techniques are presented by Sarfarazi and Haeri (2018), Zhao *et al.* (2017), and Dias and Grippon (2017).

This study investigates the stress state of bottom-hole rock using the fully coupled thermo-poroelastoplasticity model considering the effects of overburden pressure, horizontal in-situ stresses, drilling mud pressure, pore pressure and temperature on stress distribution. The bottom-hole rock can be divided into three regions according to the stress state, namely a) three directions tensile area, b) two directions compression areas and c) three directions compression area, which are classified as a) easy, b) normal and c) hard, respectively, for the corresponding fragmentation degree of difficulty.

2. Theoretical background

The formation temperature increases by increasing formation depth, as a consequence, the drilling mud has a relatively low temperature comparing to the bottom-hole rock, causing a cool effect on the bottom-hole rock. Therefore, the bottom-hole rock matrix and the pore medium will be shrunken. Moreover, the phenomenon of seepage will happen due to the pressure gradient between the drilling mud and pore fluid. Thus, it can be seen that the problem of stress distribution of bottom-hole rock is a typical Thermo-Hydro-Mechanical (THM) problem. Fig.

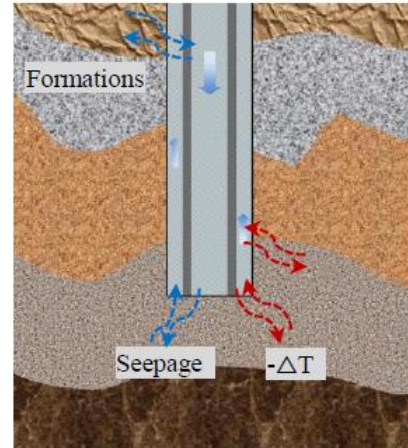


Fig. 1 The schematic of the heat transfer and seepage process

1 presents the schematic of the heat transfer and seepage process.

The THM model needs to satisfy the following three types of equations (Zhuang 2009):

1) Equilibrium Equations;

a) Conservation of mass equation for fluid

$$n \frac{\partial (S_1 \rho_1)}{\partial t} + S_1 \rho_1 \left[\frac{\partial \varepsilon_v}{\partial t} + \frac{(1-n_1)}{\rho_s} \frac{\partial \rho_s}{\partial t} \right] = -\nabla \cdot q_{r1} \quad (1)$$

where, n_1 presents the porosity of rock material, S_1 presents void saturation, ρ_s presents the density of rock matrix, ε_v is the bulk strain of rock matrix, ρ_1 is the density of pore fluid and q_{r1} is the density vector of pore fluid.

b) Energy-balance Equation

$$\frac{\partial}{\partial t} [(1-n_1)\rho_s e_s + n e_1 \rho_1] = -\nabla \cdot (I_m^k + I_1^k) \quad (2)$$

where e_s is the inner energy of unit volume of rock matrix, e_1 is the inner energy of unit volume of pore fluid, I_m^k is the average conductivity coefficient of rock matrix and pore fluid and I_1^k is the conductivity coefficient of pore fluid.

c) Momentum Conservation Equation

$$\nabla \sigma + \rho_m g = 0 \quad (3)$$

where σ is the Macroscopic total stress tensor.

2) Constitutive Equations;

a) The void saturation S_1 is the function of pore pressure P_c and temperature T .

$$S_1 = S_1(P_c, T) \quad (4)$$

b) Generalized Darcy's law

$$q_{r1} = -K(T, n_1) \cdot K_{r1} I \cdot (\nabla P - \rho_1 g \nabla z) \quad (5)$$

Where $K(T, n_1)$ representing the permeability coefficient, is function of temperature T and porosity n_1 , and K_{r1} being relative permeability, is function of saturation.

c) Density formulas for liquid and solid phases

$$\frac{\rho_1^w}{\rho_{10}^w} = 1 + \beta_{1po}(p - p_0) - \beta_{1to}(T - T_0) \quad (6)$$

$$\frac{\rho_s}{\rho_{s0}} = 1 + \frac{\bar{p} - \bar{p}_0}{K_g} - \beta_{Tg}(T - T_0) - \frac{\text{trace}(\sigma' - \sigma_0')}{(1 - n_1)3K_g} \quad (7)$$

where β_{1po} and β_{1to} are constants, ρ_1^w is the mass of unit volume of liquid phases, K_g is bulk modulus, β_{Tg} is the coefficient of thermal expansion of rock matrix and σ' represents the effective stress tensor.

The relationship between effective stress and total stress is as follows

$$\sigma' = \sigma - IS_1P \quad (8)$$

d) Stress-strain Increment Formula

$$d\sigma' = D : (d\varepsilon - I\beta_T dT + (\frac{S_1}{3K_g} + \frac{P_1}{3K_g} \frac{dS_1}{dp_1}) IdP_1 + I\beta_{sw} \frac{dS_1}{dp_1} dP_1) \quad (9)$$

3) Constraint Equations

$$P_c = P_g - P_1 \quad (10)$$

$$\varepsilon = \frac{1}{2}(\nabla u + (\nabla u)^T) \quad (11)$$

$$\varepsilon_v = \nabla \cdot u \quad (12)$$

where u represents the displacement vector and P_g is gas pressure.

According to the aforementioned equations, the basic variables of THM problem using FEM are displacement, pressure and temperature, which are function of space and time. When solving the THM problem using ABAQUS/Standard, the displacement field and seepage field are directly coupled and the temperature field is separated for indirect coupling. Therefore, the finite element form of the coupling equation of displacement field and seepage field is

$$[K]\{\bar{C}_\sigma\} - [L]\{\bar{C}_u\} = \{P\} - \{I\} \quad (13)$$

$$[B]^T \{\bar{v}\} + [H]\{\bar{u}\} = \{Q\} \quad (14)$$

where $[B]^T$ and $[L]$ are the coupled matrixes.

The difference operator is introduced as follows

$$\{\bar{\delta}_{t+\Delta t}\} - \{\bar{\delta}_t\} + \Delta t[(1 - \xi)\{\bar{v}_t\} + \xi\{\bar{\delta}_{t+\Delta t}\}] \quad (15)$$

where $0 \leq \xi \leq 1$, in order to keep the stable of numerical calculation. Using $\xi=1$, as a result, the solution is obtained as

$$\begin{aligned} [K]\{\bar{C}_\sigma\} - [L]\{\bar{C}_u\} &= \{P\} - \{I\} \\ -[B]^T \{\bar{C}_\sigma\} - \Delta t[H]\{\bar{C}_u\} & \\ &= \Delta t\{Q_{t+\Delta t}\} + [B]^T \{\bar{v}_{t+\Delta t}\} + [H]\{\bar{u}_{t+\Delta t}\} \end{aligned} \quad (16)$$

3. Plastic yield criterion of rock material

There are many models (e.g., Zhang *et al.* 2017) to describe the rock yield criteria, however, most of them require many input parameters. This paper deploys the Drucker-Prager failure criterion, which has relatively less input parameters (Zhu *et al.* 2014, Lusso *et al.* 2017, Liu *et al.* 2018, 2019).

$$F = m_a I_1 - \sqrt{J_2} + k_1 \quad (17)$$

where I_1 indicates the first stress invariant, and J_2 means the second deviatoric stress invariant.

$$I_1 = \sigma_1 + \sigma_2 + \sigma_3 \quad (18)$$

$$J_2 = \frac{1}{6} [(\sigma_1 - \sigma_2)^2 + (\sigma_1 - \sigma_3)^2 + (\sigma_2 - \sigma_3)^2] \quad (19)$$

$$m_a = \frac{2 \sin \varphi}{\sqrt{3}(3 - \sin \varphi)}, k_1 = \frac{6c \cos \varphi}{\sqrt{3}(3 - \sin \varphi)} \quad (20)$$

where φ means the angle for internal friction, c indicates the cohesion stress. $\sigma_1, \sigma_2, \sigma_3$ represent the principal stress in the cylindrical coordinate system.

4. FE Simulations and verification

4.1 FE model

The 3D simulation model of bottom-hole rock is constructed using the fully coupled thermo-poroelastoplasticity theory. The dimensional of this simulation model is 2000 mm × 2000 mm × 2000 mm, and the borehole radius is 108 mm and the depth is 1000 mm. In order to improve the calculation precision the meshes near the borehole and bottom-hole are refined meshed, the FE model is depicted in Fig. 2. The bottom of the rock model is restricted in Z direction, the left and right sides are restricted in Y direction and front, and backsides are restricted in X direction. The overburden pressure σ_z is applied on the top surface of rock model in Z direction, and the in-situ stresses of σ_H and σ_h in X and Y direction will be generated due to the lateral coefficient of rock material. Besides, these two in-situ stresses are equal because of the homogeneous of rock model. In addition, the mud pressure P_w is applied on the wellbore wall and the initial pore pressure of rock model is denoted as P_f . Another important influence factor is the temperature gradient between drilling

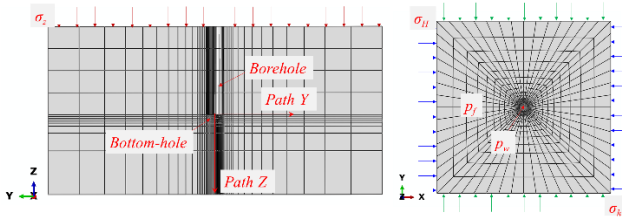


Fig. 2 The finite element model of bottom-hole and the loads applied on bottom-hole rock

Table 1 The Physical parameters of rock

Young's modulus	25406 MPa
Poisson's ratio	0.302
Permeability coefficient	$1 \times 10^{-10} \text{ m} \cdot \text{s}^{-1}$
Porosity	0.1
Solid mass density	2500 kg/m^3
Solid mass thermal expansion coefficient	$1.5 \times 10^{-5}/^\circ\text{C}$
Solid mass thermal conductivity	3.08 $\text{J}/\text{m} \cdot \text{s} \cdot ^\circ\text{C}$
Solid mass specific heat	896 $\text{J}/\text{g} \cdot ^\circ\text{C}$
Pore fluid conductivity	0.58 $\text{J}/\text{m} \cdot \text{s} \cdot ^\circ\text{C}$
Pore fluid specific heat	4200 $\text{J}/\text{g} \cdot ^\circ\text{C}$
Pore fluid expansion	$2 \times 10^{-4}/^\circ\text{C}$
Pore fluid density	1000 kg/m^3
Specific weight of pore fluid	$1 \times 10^4 \text{ N}/\text{m}^3$
Shear modulus	9756 MPa
Cohesion stress	26.13 MPa
Friction angle	24.47°
Solid bulk modulus	65000 MPa
Fluid bulk modulus	3300 MPa

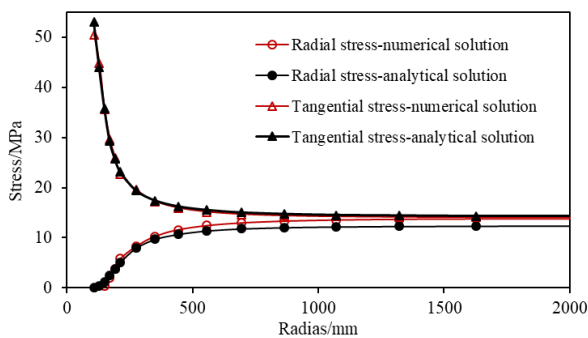


Fig. 3 The comparison with numerical solution and analytical solution

mud and formation. The wellbore wall is considered as a seepage boundary, the drilling fluid and pore fluid can be freely circulated. This means that the pore pressure at wellbore wall is equal to the drilling mud pressure and the temperature at the wellbore wall is also equal to the drilling mud temperature. In actual drilling process, when the drilling bit breaks the bottom-hole rock and the new bottom-hole is formed, as a consequence, the seepage time between drilling mud and pore fluid is short. In the simulation procedure of this study, the time is set equal to 5 seconds. In order to make the analysis conveniently, two

paths including path Y (radial) and path Z (axial) are selected as shown in Fig. 2. The physical mechanical parameters of rock specimen are mainly derived from the references (Zhu et al. 2016), and listed in Table 1.

4.2 Verification of numerical simulation model

Bradley (1979) has analyzed the stress distribution around the borehole for an elastic and homogeneous formation using the following equations.

$$\begin{aligned} \sigma_r &= \frac{\sigma_H + \sigma_h}{2} \left(1 - \frac{r_i^2}{r^2}\right) + \frac{\sigma_H - \sigma_h}{2} \left(1 - 4\frac{r_i^2}{r^2} + 3\frac{r_i^4}{r^4}\right) \cos 2\theta + \frac{r_i^2}{r^2} p_w - \alpha p(r) \\ &\quad + \delta \left[\frac{\xi}{2} \left(1 - \frac{r_i^2}{r^2}\right) - f \right] (p_w - p_f) \\ \sigma_\theta &= \frac{\sigma_H + \sigma_h}{2} \left(1 + \frac{r_i^2}{r^2}\right) - \frac{\sigma_H - \sigma_h}{2} \left(1 + 3\frac{r_i^4}{r^4}\right) \cos 2\theta - \frac{r_i^2}{r^2} p_w - \alpha p(r) \\ &\quad + \delta \left[\frac{\xi}{2} \left(1 + \frac{r_i^2}{r^2}\right) - f \right] (p_w - p_f) \\ \sigma_z &= \sigma_y - \mu \left[2(\sigma_H - \sigma_h) \frac{r_i^2}{r^2} \cos 2\theta \right] + \delta [\xi - n] (p_w - p_f) - \alpha p(r) \\ \xi &= \alpha(1 - 2\mu)(1 - \mu) \end{aligned} \quad (21)$$

where the σ_r , σ_θ , σ_z are the radial stress, tangential stress and z-axis stress respectively, and α is Biot coefficient. δ is a coefficient related to the permeability, it is equal to 1, when the wellbore wall is permeable, or equal to 0, when the wellbore wall is impermeable. $p(r)$ indicates the pore pressure at the r and p_w depicts drilling mud pressure. P_f means initial pore pressure, f expresses the porosity and μ is Poisson's ratio, and σ_H and σ_h express the maximum and minimum horizontal principal stress, respectively.

Analytical solution of stress distribution around borehole using pore-elastic model is utilized to verify numerical simulation results, as shown in Fig. 3. The results show that the numerical solutions closely agree with the analytical solutions. In the numerical simulation and analytical analysis, the temperature is not considered, neither the effect of thermo-poroelastoplasticity. The comparisons of these two types of solutions indicate the validity of numerical simulation model. The influence factors of temperature gradient and rock plastic yield will be taken into consideration in the following numerical simulation research.

5. Simulation results and analysis

5.1 The distribution of pore pressure and temperature

A thermo-poroelastoplasticity model is carried out in this section to investigate the pore pressure and temperature distribution. In this model, the drilling mud pressure is 20 MPa, overburden pressure is 75 MPa, drilling mud temperature is 60°C , initial pore pressure is 30 MPa and initial formation temperature is 90°C . The simulation results are presented in Fig. 4. The nephograms show that the pore pressure and temperature at wellbore wall is 20 MPa and 60°C , respectively, and the initial pore pressure and formation temperature is 30 MPa and 90°C , respectively. The pore pressure and temperature gradually increase away from the wellbore wall.

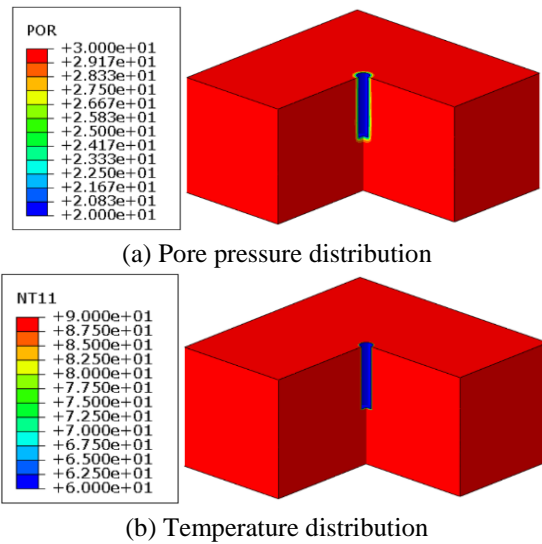


Fig. 4 The distribution of pore pressure and temperature

5.2 The influence of mud pressure

The stress condition of bottom-hole rock is sophisticated under the co-action of overburden pressure, horizontal in-situ stresses, drilling mud pressure, pore pressure and temperature, etc. The influence of mud pressure on stress distribution of bottom-hole rock is investigated in this section. The initial formation temperature is 90°C and the drilling mud temperature is 60°C and well depth is 3000 m. The Overburden pressure σ_z is obtained through the formula $\sigma_z = \rho gh$, h is the well depth, and ρ is the rock density. Therefore, in this section the overburden pressure is 75 MPa.

Fig. 5 presents the maximum/minimum principal stress distribution along the path Y under different mud pressures. The solid lines present the maximum principal stress with respect to radial distance and the dotted lines are the minimum principal stress with respect to the radial distance. The maximum principal stress of the bottom-hole rock increases by increasing drilling mud pressure. The maximum stress appears at the central of the bottom-hole rock. In contrast, the minimum principal stress appears at the junction of the bottom hole and wellbore wall. The positive value of stress illustrates the tensile stress and the negative value of stress illustrates the compressive stress. The minimum principal stress distribution shows that, when the mud pressure is zero, the stress of the central part of the bottom-hole rock is larger than zero. On the contrary, the other cases have pressure smaller than 0. The area of tensile stress state of bottom-hole rock becomes smaller by increasing mud pressure. The compressive stress area becomes larger, and the minimum principal stress at the bottom-hole totally presents a compressive stress eventually. According to the aforementioned research, the bottom-hole rock can be divided into three areas based on the stress state: a) three directions tensile area (or unidirectional compression zone, at the central part of bottom-hole), b) two directions compression area (at the outside of the central part) and c) three directions

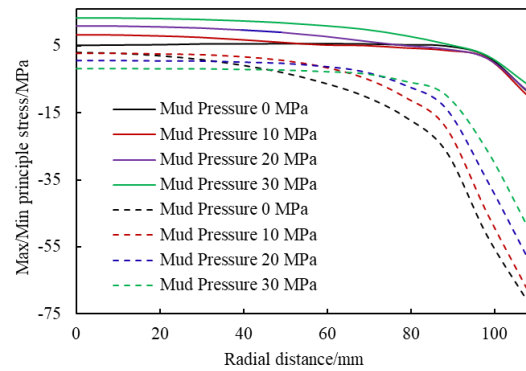


Fig. 5 The effect of mud pressure on maximum/minimum principal stress (path Y)

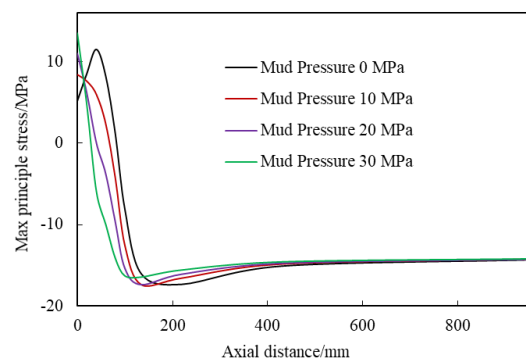


Fig. 6 The effect of mud pressure on maximum principal stress (path Z)

compression zone (the junction of the bottom-hole and wellbore wall). The central part of rock is easy to be broken, the outside of the central part rock is relatively difficult to be broken, and the junction is the most hard to be broken.

Fig. 6 illustrates the maximum principal stress distribution of bottom-hole rock in axial direction. The stress increases first and then decreases when the mud pressure is zero. The maximum principal stress at the bottom-hole surface is 5.1 MPa and increases to 11.4 MPa beneath the rock surface about 40 mm. In the underbalanced drilling, the stress decreases by increasing mud pressure, and the rock stress state changes from tensile to compressive. Fig. 7 presents the maximum principal stress nephogram. The high stress state area decreases with increasing mud pressure, which mainly caused by the mud pressure hold effect. The maximum principal stress at bottom-hole surface is increasing by increasing mud pressure because the larger mud pressure will lead to high pore pressure of bottom-hole rock.

5.3 The influence of well depth

In order to investigate the influence of well depth on stress distribution of bottom-hole rock, the differential pressure between pore pressure and mud pressure is kept constant at 10 MPa, and the temperature gradient is kept constant at 30°C. Fig. 8 shows the maximum/minimum principal stress values with respect to radial distance of path

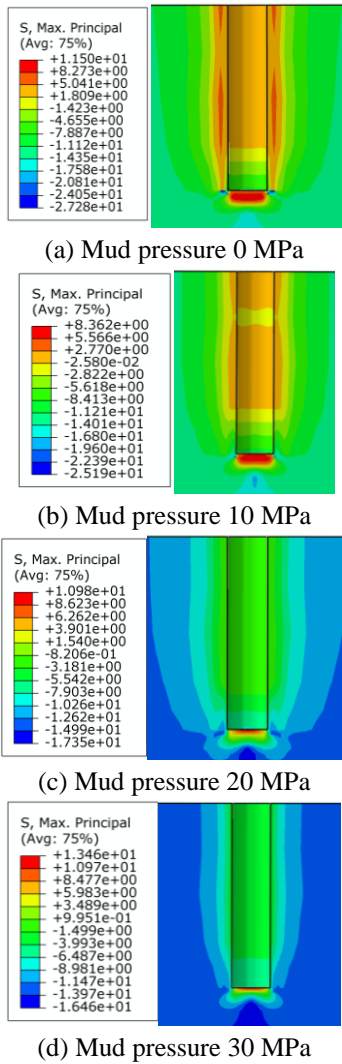


Fig. 7 The maximum principal stress distribution of bottom-hole rock under different mud pressures

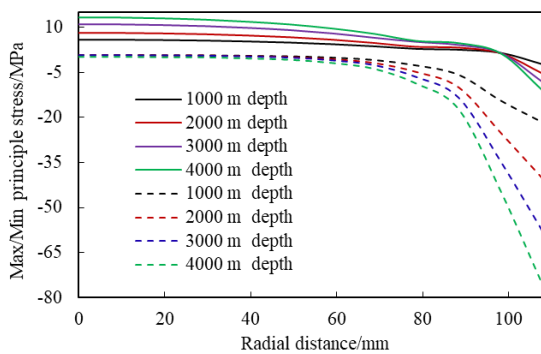


Fig. 8 The effect of well depth on maximum/minimum principal stress (path Y)

Y. The maximum principal stress of the bottom-hole increases with increasing well depth. This is mainly because the increase of well depth causes an increase in the mud pressure because the differential pressure is constant. As a result, the pore pressure increases and causes the tensile stress of rock matrix to increase. The minimum principal stress of central part of bottom-hole rock is almost

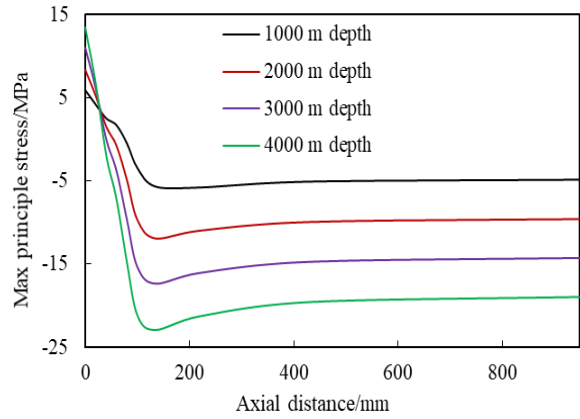
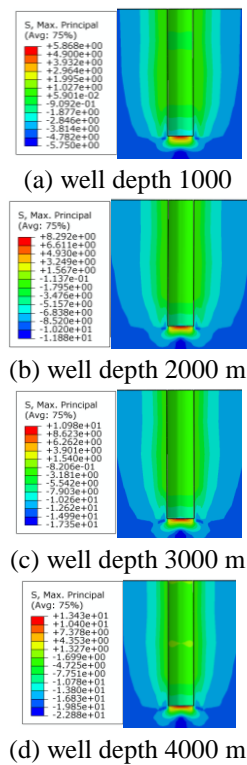


Fig. 9 The effect of well depth on maximum principal stress (path Z)



independent of well depth, but it decreases rapidly near the wellbore wall and the larger the well depth is, the smaller the stress will be.

Fig. 9 shows the maximum principal stress of bottom-hole rock in path Z direction. The maximum principal stress of the rock beneath bottom within certain distance increases by increasing well depth, which mainly cause by the increase of mud pressure. Fig. 10 presents the maximum principal stress nephogram under different well depths.

Air drilling is a special approach used in nowadays oil gas exploration. In air drilling process, the hold pressure on bottom-hole rock almost equals to zero. Fig. 11 presents the maximum principal stress distribution of the bottom-hole in path Z direction associated with different well depth. In the simulation procedure, the temperature gradient is kept constant at 30°C. It is illustrated that, the maximum principal stress first increases then decreases and keeps at a

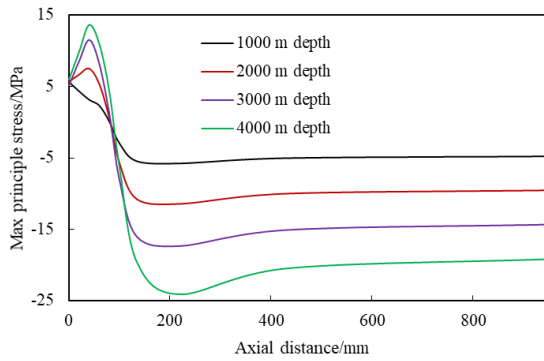


Fig. 11 The maximum principal stress with respect to axial distance

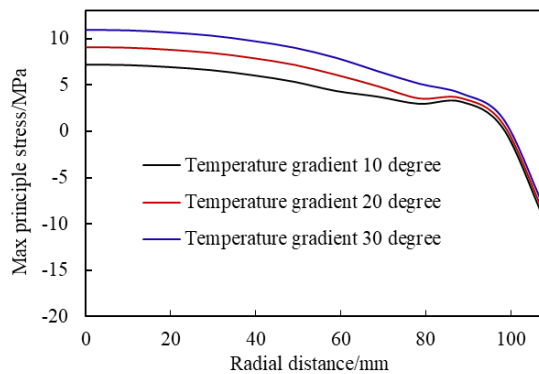


Fig. 12 The distribution of maximum principal stress under various temperature gradients (path Y)

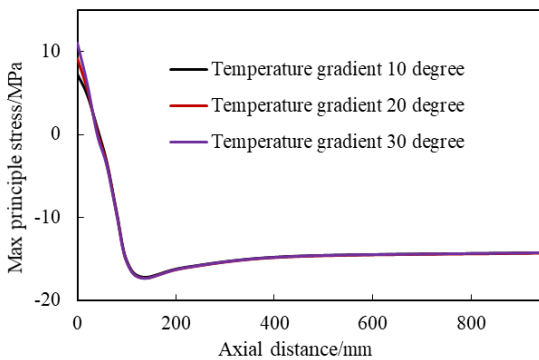
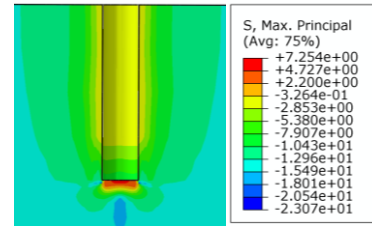


Fig. 13 The distribution of maximum principal stress under various temperature gradients (path Z)

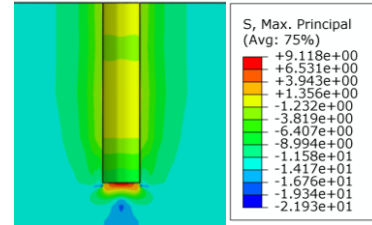
stable state eventually with respect to axial distance. The maximum principal stress at bottom-hole surface is almost independent of well depth because the pressure applied on the rock surface is always zero. Instead, the maximum principal stress at a certain distance beneath the bottom-hole is increasing with the well depth, which indicates that in gas drilling, the bottom-hole rock is easier to be broken than in deeper wells.

5.4 The influence temperature difference

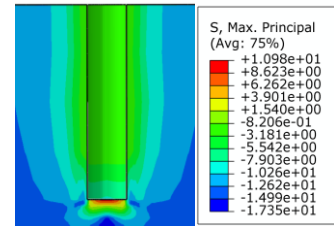
Figs. 12 and 13 plot the maximum principal stress distribution in path Y and path Z under different



(a) temperature gradient 10 degree



(b) temperature gradient 20 degree



(c) temperature gradient 30 degree

Fig. 14 The maximum principal stress distribution nephogram of bottom-hole rock under different temperature gradients

temperature gradients, respectively. The maximum principal stress increases by increasing temperature gradient, which is beneficial to rock fragmentation. Moreover, the influence of temperature on bottom-hole rock stress disappears beneath a certain distance in the axial direction of bottom-hole rock. The influenced area is related to the heat transfer coefficient of rock matrix and pore fluid, heat conduction time and other factors. Fig. 14 shows the maximum principal stress distribution nephogram of bottom-hole rock under different temperature gradients.

6. Conclusions

This study investigated the stress distribution problem in the underbalanced drilling, and the above analysis supported the following conclusions.

- During gas drilling, the maximum principal stress first increases then decreases and keeps at a stable state eventually with respect to axial distance. The maximum principal stress at bottom-hole surface is almost independent of well depth because the pressure applied on the rock surface is always zero. Instead, the maximum principal stress at a certain distance beneath the bottom-hole is increasing with the well depth, indicating that the bottom-hole rock is easier to be broken in deeper wells.

- The maximum principal stress increases by increasing temperature gradient, which is beneficial to rock fragmentation. The influence of temperature on bottom-hole

rock stress disappears beneath a certain distance in axial direction of bottom-hole rock. The influenced area is related to the heat transfer coefficient of rock matrix and pore fluid, heat conduction time and other factors.

- The bottom-hole rock can be divided into three areas based on the stress state, namely, a) three directions tensile area (or unidirectional compression zone, at the central part of bottom-hole), b) two directions compression area (at the outside of the central part) and c) three directions compression zone (the junction of the bottom-hole and wellbore wall). The central part of rock is easy to be broken, the outside of the central part rock is relatively difficult to be broken, and the junction is most hard to be broken.

Acknowledgements

This study is supported by the China Postdoctoral Science Foundation (2018M633403), Scientific Research Starting Project of SWPU (2018QHZ015), Applied Basic Research of Sichuan Province (Free Exploration-19YYJC2783), National Natural Science Foundation of China (51674214), Youth Science and Technology Innovation Research Team of Sichuan Province (2017TD0014). Such supports are greatly appreciated by the authors.

References

- Amadi, W.K. and Iyalla, I. (2012), "Application of mechanical specific energy techniques in reducing drilling cost in deepwater development", *Proceedings of the SPE Deepwater Drilling and Completions Conference*, Galveston, Texas, U.S.A., June.
- Aminul, I.M., Skalle, P. and Benjamin, P. (2009b), "Analytical and numerical study of consolidation effect on time delayed borehole stability during underbalanced drilling in shale", *Proceedings of the Kuwait International Petroleum Conference and Exhibition*, Kuwait City, Kuwait, December.
- Aminul, I.M., Skalle, P. and Evgeniy, T. (2009a), "Underbalanced drilling in shale-perspective of factors influences mechanical borehole instability", *Proceedings of the International Petroleum Technology Conference*.
- Azeemuddin, M., Maya, D.A. and Guzman, E. (2006), "Underbalanced drilling borehole stability evaluation and implementation in depleted reservoirs", *Proceedings of the IADC/SPE Drilling Conference*, Miami, Florida, U.S.A., February.
- Bezminabadi, S.N., Ramezanzadeh, A., Jalali, S.M.E., Tokhmechi, B. and Roustaei, A. (2017), "Effect of rock properties on ROP modeling using statistical and intelligent methods: A case study of an oil well in Southwest of Iran", *Arch. Min. Sci.*, **62**(1), 131-144.
- Bradley, W.B. (1979), "Failure of inclined boreholes", *J. Energy Res. Technol.*, **101**(4), 232-239.
- Chang, D., Li, G., Shen, Z., Huang, Z., Tian, S., Shi, H. and Song, X. (2014), "A study on the effect of bottom-hole differential pressure on the rock stress field", *Part A: Recov. Utilizat. Environ. Eff.*, **36**(3), 275-283.
- Dias, D. and Gripton, J. (2017), "Numerical modelling of a pile-supported embankment using variable inertia piles", *Struct. Eng. Mech.*, **61**(2), 245-253.
- He, S., Wang, W., Tang, M., Hu, B. and Xue, W. (2014), "Effects of fluid seepage on wellbore stability of horizontal wells drilled underbalanced", *J. Nat. Gas Sci. Eng.*, **21**, 338-347.
- Li, G., Chang, D., Shen, Z., Huang, Z., Tian, S., Shi, H. and Song, X. (2016), "Study of the bottom-hole rock stress field under water jet impact", *Energy Sources, Part A: Recov. Utilizat. Environ. Eff.*, **38**(2), 164-173.
- Li, J., Guo, B., Yang, S. and Liu, G. (2014), "The complexity of thermal effect on rock failure in gas-drilling shale-gas wells", *J. Nat. Gas Sci. Eng.*, **21**, 255-259.
- Li, X.B., Dou, T.W. and Dong, D.R. (2011), "Stress state of bottom hole rocks in underbalanced drilling", *Acta Petroleol Sinic.*, **32**, 329-334.
- Liu, W., Qian, X., Li, T., Zhou, Y. and Zhu, X. (2019), "Investigation of the tool-rock interaction using Drucker-Prager failure criterion", *J. Petrol. Sci. Eng.*, **173**, 269-278.
- Liu, W., Zhu, X. and Jing, J. (2018), "The analysis of ductile-brittle failure mode transition in rock cutting", *J. Petrol. Sci. Eng.*, **163**, 311-319.
- Lusso, C., Ern, A., Bouchut, F., Mangeney, A., Farin, M. and Roche, O. (2017), "Two-dimensional simulation by regularization of free surface viscoplastic flows with drucker-prager yield stress and application to granular collapse", *J. Comput. Phys.*, **333**, 387-408.
- McLellan, P. and Hawkes, C. (2001), "Borehole stability analysis for underbalanced drilling", *J. Can. Petrol. Technol.*, 4031-4038.
- Nguyen, V.P., Lian, H., Rabczuk, T. and Bordas, S. (2017), "Modelling hydraulic fractures in porous media using flow cohesive interface elements", *Eng. Geol.*, **225**, 68-82.
- Qiu, K.B., Gherryo, Y. and Marsden, R. (2008), "Underbalanced drilling of a horizontal well in depleted reservoir: A wellbore-stability perspective", *Proceedings of the SPE Middle East Oil and Gas Show and Conference*, Manama, Bahrain, March.
- Rabczuk, T. and Ren, H.A. (2017), "A peridynamics formulation for quasi-static fracture and contact in rock", *Eng. Geol.*, **225**, 42-48.
- Roshan, H. and Rahman, S.S. (2011), "3D borehole model for evaluation of wellbore instabilities in underbalanced drilling", *Proceedings of the SPE EUROPEC/EAGE Annual Conference and Exhibition*, Vienna, Austria, May.
- Rumzan, I. and Schmitt D.R. (2001), "The influence of well bore fluid pressure on drilling penetration rates and stress dependent strength", *Rock Mech. Nat. Inter.*, **1**, 911-917.
- Salehi, S. and Hareland, G. (2007), "Wellbore stability analysis in UBD wells of Iranian fields", *Proceedings of the 1st EAGE International Petroleum Conference and Exhibition*, Shiraz, Iran, May.
- Salehi, S., Hareland, G. and Nygaard, R. (2010), "Numerical simulations of wellbore stability in under-balanced-drilling wells", *J. Petrol. Sci. Eng.*, **72**, 229-235.
- Sarfarazi, V. and Haeri, H. (2018), "Three-dimensional numerical modeling of effect of bedding layer on the tensile failure behavior in hollow disc models using particle flow code (PFC3D)", *Struct. Eng. Mech.*, **68**(5), 537-547.
- Sarfarazi, V., Haeri, H., Shemirani, A.B. and Nezamabadi, M.F. (2018), "A fracture mechanics simulation of the pre-holed concrete Brazilian discs", *Struct. Eng. Mech.*, **66**(3), 343-351.
- Shirkavand, F., Hareland, G. and Aadnoy, B.S. (2009), "Rock mechanical modelling for a underbalanced drilling rate of penetration prediction", *Proceedings of the 43rd Conference on US Rock Mechanics Symposium and the 4th Conference on US-Canada Rock Mechanics Symposium*, Sheville, North Carolina, U.S.A., June-July.
- Zhang, H., Wan, Z., Wang, C., Ma, Z., Zhang, Y. and Cheng, J. (2017), "A statistical damage constitutive model for geomaterials under plane-strain biaxial stress state", *Adv. Math. Phys.*

- Zhang, H., Gao, D., Salehi, S. and Guo, B. (2013), "Effect of fluid temperature on rock failure in borehole drilling", *J. Eng. Mech.*, **140**(1), 82-90.
- Zhang, H., Zhang, H., Guo, B. and Gang, M. (2012), "Analytical and numerical modeling reveals the mechanism of rock failure in gas UBD", *J. Nat. Gas Sci. Eng.*, **4**, 29-34.
- Zhao, H.L., Liu, X., Bao, Y.H. and Yuan, Y. (2017), "Nonlinear simulation of tunnel linings with a simplified numerical modelling", *Struct. Eng. Mech.*, **61**(5), 593-603.
- Zhou, S., Zhuang, X. and Rabczuk, T. (2018b), "A phase-field modeling approach of fracture propagation in poroelastic media", *Eng. Geol.*, **240**, 189-203.
- Zhou, S., Zhuang, X., Zhu, H. and Rabczuk, T. (2018a), "Phase field modelling of crack propagation, branching and coalescence in rocks", *Theoret. Appl. Fract. Mech.*, **96**, 174-192.
- Zhu, X., Liu, W. and Zheng, H. (2016), "A fully coupled thermo-poroelastoplasticity analysis of wellbore stability", *Geomech. Eng.*, **10**(4), 437-454.
- Zhu, X.H., Liu, W.J. and Liu, Q.Y. (2014), "The mechanism and law of wellbore instability due to drill string impact in air drilling", *Int. J. Oil Gas Coal Technol.*, **8**(2), 153-181.
- Zhuang, X., Huang, R., Liang, C. and Rabczuk, T. (2014), "A coupled thermo-hydro-mechanical model of jointed hard rock for compressed air energy storage", *Math. Probl. Eng.*
- Zhuang, Z. (2009), *Finite Element Analysis and Application Based on ABAQUS*, Tsinghua University Press.